

RXTE Observations of an Outburst of Recurrent X-ray Nova GS 1354–644

Mikhail G. Revnivtsev^{1,2}, Konstantin N. Borozdin^{2,1}, William C. Priedhorsky², Alexey Vikhlinin³

¹ – Space Research Institute, Moscow, Russia

² – Los Alamos National Laboratory, Los Alamos, NM 87545, USA

³ – Harvard-Smithsonian Center for Astrophysics, Cambridge, MA 02138, USA

ABSTRACT

We present the results of Rossi X-ray Timing Explorer observations of GS 1354–644 during a modest outburst in 1997–1998. The source is one of a handful of black hole X-ray transients that are confirmed to be recurrent in X-rays. A 1987 outburst of the same source observed by Ginga was much brighter, and showed a high/soft spectral state. In contrast the 1997–1998 outburst showed a low/hard spectral state. Both states are typical of black hole binaries. The RXTE All Sky Monitor observed an outburst duration of 150 to 200 days. PCA and HEXTE observations covered ~ 70 days near the maximum of the light curve and during the flux decline. Throughout the observations, the spectrum can be approximated by Compton upscattering of soft photons by energetic electrons. The hot electron cloud has a temperature $kT \sim 30$ keV and optical depth $\tau \sim 4$ –5. To fit the data well an additional iron fluorescent line and reflection component are required, which indicates the presence of optically thick cool material, most probably in the outer part of the accretion disk. Dramatic fast variability was observed, and has been analyzed in the context of a shot noise model. The spectrum appeared to be softest at the peaks of the shot-noise variability. The shape of the power spectrum was typical for black hole systems in a low/hard state. We note a qualitative difference in the shape of the dependence of fractional variability on energy, when we compare systems with black holes and with neutron stars. Since it is difficult to discriminate these systems on spectral grounds, at least in their low/hard states, this new difference might be important.

1. Introduction

A modest X-ray outburst from the recurrent transient X1354–644 was detected by the All Sky Monitor (ASM) aboard the Rossi X-ray Timing Explorer (RXTE) around 1

November 1997 (Remillard, Marshall & Takeshima 1998). The flux from the source as measured by the ASM in the 2-12 keV energy band, rose gradually to 40-50 mCrab in mid-November, stayed at this level for about a month, then started a slow decline. The maximum hard X-ray flux observed by BATSE (Harmon & Robinson 1998) and HEXTE (Heindl et al. 1997) appeared to be around 150 mCrab, indicating a hard spectrum. HEXTE detected an exponential spectral cutoff at higher energies.

Castro-Tirado (1997) obtained B- and R-band images following the detection of the source in X-rays. The optical counterpart BW Cir was found to be in a bright state. Radio (Fender et al. 1997) and infrared (Soria, Bessell & Wood 1998) emission was also detected during the X-ray outburst. Spectroscopic observations obtained in January 1998, reveal a strong H-alpha line in emission, with a profile that varied from double- to single-peaked over three nights, reminiscent of the black hole microquasar GRO 1655-40 during its 1996 outburst, and strongly suggesting an accretion disk origin (Buxton et al. 1998).

The X-ray transient source X1354–644 belongs to the class of X-ray binaries known as X-ray Novae (e.g. Sunyaev et al. 1994; Tanaka & Shibazaki 1996). All sources in this class are assumed to be recurrent, but only a few have been observed in more than one X-ray outburst. In case of X1354–644, thanks to observations of a common optical counterpart (Pedersen, Ilovaisky & van der Klis 1987, Castro-Tirado et al. 1997), one can reliably identify the 1997 X-ray event with one observed by Ginga in 1987 as GS 1354–64 (Makino 1987, Kitamoto et al. 1990). It is quite probable that X-ray emission from the same source, under different names, was detected also in 1967 (Harries et al. 1967, Francey 1971), in 1971-1972 (Markert et al. 1977), and in 1974-1976 (Seward et al. 1976; Wood et al. 1984). Those earlier observations however are more disputable because of relatively poor (\sim degrees) localization for the X-ray source and the lack of counterpart detections at other wavelengths.

Different outbursts of the source varied substantially in peak flux. The most prominent outburst from this area of sky was detected in 1967 as Cen X-2 (Harries et al. 1967). It was the first X-ray transient found, and still one of the brightest Galactic X-ray sources known. Its association with GS 1354–644 is however questionable because of poor position determination for Cen X-2, and because the 1967 outburst luminosity would have been much higher than Eddington. The peak fluxes detected by Ginga in 1987 (Kitamoto et al. 1990) and by OSO-7 in 1971-1972 (Markert et al. 1977) were about 2 orders of magnitude weaker than Cen X-2. The maximum flux detected by RXTE in 1997 was about 3 times lower than in 1987 outburst.

The energy spectra were also quite different for the two outbursts (1987 and 1997). The spectrum measured with Ginga in 1987 was composed of a strong soft component

below 10 keV and a power law at higher energies, which is typical for black-hole binaries in their “high” spectral state. In contrast, the spectrum detected by RXTE in the current outburst is typical of the “low” spectral state of Galactic X-ray binaries.

In this paper we present an analysis of the observations of GS 1354–644 during its 1997–1998 outburst based on RXTE data. An overview of observations and our data reduction approach are presented in section 2. Our timing analysis is presented in §3, and spectral analysis in §4. We compare our results with other sources and with some theoretical models in section 5. We summarize our results in §6.

2. Observations and data reduction

The Rossi X-ray Timing Explorer satellite (Bradt, Rothschild & Swank 1993) has two coaligned spectrometers the PCA and HEXTE, with narrow fields of view, as well as an All Sky Monitor (ASM). PCA and HEXTE together provide broad band spectral coverage in the energy range from 3 to ~ 200 keV. The ASM tracks the long term behavior of sources in the 2–12 keV energy band. The data for our analysis have been obtained from the RXTE Guest Observer Facility at GSFC, which is a part of High Energy Astrophysics Science Archive Research Center (HEASARC).

The reduction of PCA and HEXTE data was performed with the standard *ftools* package. To estimate the PCA background we applied the *L7/240* background model, which takes into account various particle monitors and the SAA history, for the 17 November 1998 observation, and the *VLE* (Very Large Events) -based model for other observations.

We used PCA response matrix v.3.3 (Jahoda 1998 a, b). Analysis of the Crab nebula spectra confirmed that the systematic uncertainties of the matrix were less than 1% in the 3–20 keV energy band. Uncertainties in the response, and a sharp decrease of PCA effective area below 3 keV, makes it hard to accurately measure low-energy spectral absorption. We have used PCA data only in the 3–20 keV range, and added 1% systematic error for each PCA channel to account for residual uncertainties in the spectral response. All spectra were corrected for dead-time as per Zhang & Jahoda (1996).

Response matrix v.2.6 was used to fit the HEXTE spectra (Rothschild et al. 1998). The background value for each cluster of HEXTE detectors was estimated from adjacent off-source observations. An upper energy limit for the analysis was defined according to the brightness of the source. Typically, we did not consider data at energies higher than $\sim 150 - 200$ keV, where background subtraction uncertainties became unacceptably large. A dead time correction was applied to all observations.

The pointed RXTE observations are summarized in Table 1. The 1997 PCA and HEXTE observations were carried out near outburst maximum and adjacent rise and decline phases. During the observation of Nov 1998 the source was much dimmer, probably at or approaching quiescence.

3. Variability

3.1. Light curve of the outburst

The 1997 light curve showed a triangular profile, possibly with a short plateau near maximum, similar to that observed from other X-ray transients (e.g. Lochner & Roussel-Dupre 1994; Harmon et al. 1994). For general light curve morphologies see Chen, Shrader & Livio 1997.

The light curve of the source measured by the ASM in the 2-12 keV energy band is presented in Fig.1. When approximated by an exponential function, the rise time parameter is 20 ± 2 days and decay time parameter around 40 days. Flux measurements by the PCA in the 2-30 keV energy band and by HEXTE in the 20-100 keV energy band are shown at the same Figure. There is some evidence for a secondary maximum or “kick”, typical for outbursts of X-ray Novae (e.g. Sunyaev et al. 1994; review in Tanaka & Shibazaki 1996). The light curve of the previous outburst of this source, tracked by the Ginga ASM, had a plateau and a decline with time scales around 60 days (Kitamoto et al. 1990). The peak flux of the 1997-1998 outburst in the 1-10 keV band extrapolated from PCA measurements was $\sim 1.1 \times 10^{-9}$ erg s $^{-1}$ cm $^{-2}$, which is almost three times lower than the maximum flux detected with Ginga in 1987 (Kitamoto et al. 1990).

3.2. Fast variability

The PCA detected a strong flux variability as illustrated by Fig.2. The source flux varied by a factor of 2-3 in 10 to 20 s. Such variability is often fit by shot noise models (Terrell 1972), in which the light curve is made up of randomly occurring discrete and identical events, the “shots”. The approach was further developed (Sutherland, Weisskopf & Kahn 1978), and has been proven to be quite useful in interpreting the archetypical black hole candidate Cyg X-1 (Lochner, Swank & Szymkowiak 1991) and other black hole binaries in their low state. We shall discuss below the application of this model to GS 1354–644.

Another method to study fast variability is by means of Fourier techniques (see

the detailed discussion in van der Klis 1989), in particular, by the analysis of the power density spectra (PDS). PDSs measured with the PCA for GS 1354–644 can be qualitatively described as the sum of at least two band-limited components, each of which is a constant below its break frequency, and a power-law with a slope ~ -2 above its break frequency. PDSs for observations #3 and #9 are shown in Fig.3. The power spectra have been normalized as squared fractional *rms*, according to Belloni & Hasinger (1990), and rebinned logarithmically in frequency. Rudimental white-noise was subtracted. It was estimated by Poissonian statistics as modified by dead-time effects. We have plotted PDSs as $f \times \left(\frac{rms}{mean}\right)^2$ vs. frequency. As was argued, e.g. by Belloni et al. (1997), this convention has important advantages, namely, a plot gives a direct visual idea of the power distribution, and Lorentzian functions representing band-limited noise are symmetric in a log-log plot. This convention was used only for the plot, while all analytic fits (see below) were performed on the original power spectra.

We fitted the PDS by a sum of functions $\sim \frac{1}{1+(\frac{f}{f_{br}})^2}$, each of which represents the power spectrum from single type of exponential shots with a profile $s(t) \sim \exp(\frac{-(t-t_0)}{\tau})$, for $t > t_0$, $\tau = 1/(2\pi f_{br})$. The PDSs for observations #5–9 are fitted satisfactorily by two such components, but for the first four observations a third, intermediate, component should be included for a good representation of the data. The fitting parameters are presented on Table 2. The inferred parameters are very similar to those detected for other black holes (e.g. Nowak et al. 1999a; Nowak, Wilms & Dove 1999; Grove et al. 1998) and neutron stars (e.g. Olive et al. 1998a) in their low state. The frequency of the first break in the PDS evolved significantly with time - it appeared at its lowest frequency near the outburst maximum, and shifted to higher frequencies with time. The frequency of the last break, however, remained fairly stable.

The energy-resolved power density analysis showed that the f_{break} frequencies do not vary significantly with energy, similar to what is observed for Cyg X-1 (e.g. Nowak, Wilms & Dove 1999) and other black hole candidates.

The dependence of integrated fractional variability on energy in the full analyzed frequency range (10^{-3} –50 Hz) is presented in Fig.4a (in *rms* percent). The decline of integrated *rms* with energy will be discussed in more detail in the next section, and compared with data from other sources in section 5.3.

3.3. Shot noise model

Strong chaotic variability has been detected in many Galactic binaries in their hard/low spectral state. Following the approach developed by Terrell (1972), such variability can be modeled in terms of a shot noise model (e.g. Lochner, Swank & Szymkowiak 1991 and references therein). In the shot noise model, the light curve is assumed to be composed of a number of individual shots or microflares. In principle, different shots might influence each other, and might have various shapes and spectra. However the models are usually simplified to reduce the number of free parameters. We typically assume that there are only a few types of shots, and that all shots of a given type are identical. In this simplified model statistical analyses of the observed light curve allow the determination of shot parameters. For GS 1354–644, the overall shape of the power density spectrum suggests that the light curve is formed by two or three different types of shots with characteristic times corresponding to the breaks in PDS, $\tau = 1/(2\pi f_{br})$ (see Table 2).

The power density spectrum does not provide a complete description of the shots, because it is not possible to determine independently shot rates and their intensities. To obtain additional information we analyzed the flux histogram. The probability histogram for the flux values integrated into 16-sec bins is presented in Fig.5. We selected 16-sec time bins to study the long shots. The PDS shows that long shots and short shots give almost equal input into the integrated fractional variability of the source, but the contribution of short shots to the source variability is negligible below about 0.1 Hz. The number of short shots in each 16-sec bin is large enough that their contribution is nearly constant. To avoid the influence of Poissonian counting statistics on the distribution, we have chosen the flux bins to be 2 times wider than the Poissonian error associated with each bin.

For high shot rates one would expect that the distribution, according to the central limit theorem, would have a symmetrical Gaussian shape. However, this is not the case for our distribution, which has a detectable deficit at lower fluxes. This shape suggests a low shot rate, and can be fitted by a Poissonian distribution, if the duration of any single shot is substantially shorter than the 16-second bin width. For GS 1354–644 the first PDS component corresponds to time scales of 2-5 seconds, while the flux has been integrated into 16-sec bins. We have assumed that the total flux from the source is a sum of a constant component, which is stable on the time scale of one observation, and a variable component formed by individual shots. As was mentioned above, short shots appear as part of the constant component, so the flux variations are caused by long shots only. We have fitted the flux density distribution as a sum of constant and variable components by applying the maximum likelihood method, which is preferable to chi-square statistics for low event rates. The best fit for the shot rate was $\simeq 0.3$ shots per second, and the best fit for constant

component was in the range of 50–70% of the total flux. The signal detected from an individual shot was estimated to be ~ 500 PCA counts for the first observation of 1997, and ~ 200 PCA counts for the last outburst observation (#9). The best fit obtained for observation #4 is presented in Fig.5. We repeated the analysis for a 64-sec integration time and obtained consistent results. The low shot rate for long shots shows that the variability of the source on time scales of tens of seconds is caused by relatively rare powerful flares.

Unfortunately, we were not able to study the contribution of short shots by the same method, because the flux distribution for time scales of tenths of a second depends strongly on both the short and long shots. However, the integrated *rms* variability of the short shots, combined with some simple constraints on the shot amplitude, allows us to estimate the shot overlapping parameter (see Vikhlinin et al. 1995 for the method description), and consequently derive the shot rate. The short shot rate can be estimated to be ~ 10 -15 shots/s.

The physical origin of the shots is not very clear. For GS 1354–644, as well as for other black hole systems in their low state, the break frequencies detected in PDS (~ 1 Hz) are much lower than would be expected for the environment close to a stellar mass black hole ($\sim 10^3$ Hz). The shape of the energy spectrum, which is dominated by the Comptonized emission component, moves us to explore whether the Comptonization might be responsible for the time blurring of intrinsically short shots. (This could be the case if the product of the Compton optical depth and light crossing time is of order one second). The detected dependence of fractional variability on energy (Fig.4a) at first glance seems to support this interpretation, because photons of higher energy undergo on average more interactions and so must have a wider distribution in time and lower integral variability. However, the fractional variability integrated up to the lowest break in PDS should not be affected by this mechanism and should therefore be independent of the energy. We tried to test this assumption for GS 1354–644, but found that slope of the dependence of *rms* variation vs energy for the frequencies below 0.02 Hz (see Fig.4b) cannot be defined accurately. To get a more definitive answer we had to repeat our analysis for a much brighter source, Cyg X–1, which in many ways resembles GS 1354–644. For Cyg X–1 we can clearly see that the fractional variability decreases with energy both when integrated up to 50 Hz, and when integrated for the frequency range below 0.2 Hz. This last result is in direct contradiction with an assumption that the Compton up-scattering is responsible for the low-state PDS break frequencies.

3.4. Time lags in GS 1354-644

Another way to study rapid fluctuations in the flux is to compute time lags between variations in different energy bands. We calculated frequency-dependent phase lags according to the procedure of Nowak et al. (1999a). Due to the faintness of the source we were forced to sum almost all of the data available – from observations #2 through #9 – to obtain a significant result. The total integrated live time for these PCA observations was ~ 48 ksec. Time lags are presented in Fig. 6. The error values were estimated from the width of the lag distribution histogram. One can see that, at least qualitatively, the dependence of phase lag on Fourier frequency is very similar to low states in other X-ray binaries, both in black holes and neutron stars (e.g. Nowak et al. 1999a, Grove et al. 1999, Ford et al. 1999).

4. Energy spectrum

The energy spectrum of GS 1354–644 during its 1997 outburst can be roughly represented as a hard power law with slope $\alpha \sim 1.5$, and a high-energy cutoff above ~ 50 keV. Such spectra are typical for black hole binaries in the low/hard spectral state. A commonly accepted mechanism for generating the hard radiation in this state is thermal Comptonization (Shapiro, Lightman & Eardley 1976; Sunyaev & Titarchuk 1980). Applying a thermal Comptonization model to the hard-state BH spectra, one infers a hot cloud surrounding the central object (BH) with typical plasma temperature ~ 50 keV and a Thomson optical depth $\gtrsim 1$. Such a cloud can Comptonize the soft photons from the central region, most likely from an accretion disk.

We fit the spectrum with a variety of models, ranging from a simple power law to detailed Comptonization, in search of the underlying physics. The results are presented in Tables 3 and 4. We present results for two groups of observations (2-5 and 6-9), because the spectral parameters did not differ significantly within each group, but summing the groups allows a more accurate parameter estimates. The spectra for observations 2-5 and also for observation #10 are presented in Fig.7. The y-axis is in units of the photon flux multiplied by the energy squared. These units show directly the energy content per decade. Crab Nebula spectrum plotted the same way would be close to flat, and Galactic black hole binaries typically show a negative slope in their high state, and a positive slope (up to ~ 100 keV) in their low state.

On using the same models for the PCA and HEXTE data considered jointly we found that cross-calibration uncertainties of these instruments played a significant role. Namely,

any power law (with high energy cutoff) approximations gave noticeably different photon index values, even if the same energy bands were used. So we used power laws with photon indexes differing by 0.08-0.1 for PCA and HEXTE spectra (we followed here an approach by Wilms et al. 1999). In the Table 3 we present the PCA photon indices.

The fits show a noticeable high energy cut-off at energies above ~ 60 keV. While different models give different cut-off parameters, no fit without a cut-off was satisfactory. In fact, the spectrum cannot be fully described by a simple power law, with or without a high energy cut-off. The spectral fit is improved significantly by adding a neutral iron fluorescent line and a reflection component, which indicates that some part of the emission is reflected by optically thick cold material, most probably in the outer accretion disk (Basko, Sunyaev & Titarchuk 1974; George & Fabian 1991; Magdziarz & Zdziarski 1995). This component was represented by *peirav* model of *XSPEC* package, which simulated reflection from a neutral medium.

For Comptonization models, we applied the classical *compST* model of Sunyaev & Titarchuk 1980, and the more recent generalized *compTT* model (Titarchuk 1994). For both cases the parameter E_{cut} , the cutoff energy, has been frozen at the value $3kT_e$, where kT_e is the temperature of the Comptonizing hot electrons. The value of the optical depth parameter depends on the assumed geometry - for *compTT* we cite the τ parameter for both spherical and disk geometries. It is well known that the cut-off at energies higher than $\sim 3kT_e$ is more abrupt in the spectrum of Comptonized emission than a simple exponential cut-off, but we were not able to detect a statistically significant difference between these two cut-off models because of the faintness of the source. A Gaussian component with the central energy 6.4 keV and FWHM equal to 0.1 keV (frozen at these values) was added to account for emission at the iron line.

During the observation of 17 November 1998 (# 10) the PCA measured a very low flux. The spectrum was found to be softer, with a power law photon index ~ 2 in comparison with ~ 1.5 the year before. This observation might represent the quiescent state of GS 1354–644 or the transition to quiescence.

4.1. Spectral change analysis

To study spectral changes in more detail, we analyzed raw spectral ratios. This method is based on the idea that, if one divides one spectrum by another, subtle differences between two are evident in the ratio. We applied this method to spectra obtained during different PCA observations and also to spectra collected within each observation, segregated by flux

level. In all cases, the spectral ratios could be approximated by a single power law E^β in spite of the complexity of the initial spectra. We have used the power law index β for quantitative comparisons of spectral ratios. We labeled this index as β_1 when the method was applied to different observations, and β_2 when we compared high-flux and low-flux spectra for the same observation. In both cases we call β spectral ratio slope or differential slope.

For the separate observations, we divided each spectrum by the spectrum of the observation with maximum flux (#4). This method allowed us to exclude from the analysis uncertainties in the PCA response matrix, and hence to study fine differences between spectra. The drift of detector parameters, however, can contribute a significant systematic error, if the interval between observations is too long. To estimate the level of such systematic errors, we applied the same technique to Crab spectra taken before, during and after the outburst of GS 1354–644. The apparent changes in the Crab spectral ratio caused by drifting detector response are much smaller than the changes seen in GS 1354–644 (Fig.8). The X-ray spectrum of GS 1354–644 became softer with time, then suddenly harder for observation #9. There is no clear correlation with flux level. Instead, observations at the same flux level taken during rise and decline had significantly different spectral ratios (see differential slopes β_1 on Table 5).

The same technique was applied to study the relation between spectrum and flux within each observation. In this case the data were segregated according to the total count rate averaged into 16-sec bins. The range from minimum to maximum flux was divided into three equal parts, and two spectra for “high” and “low” fluxes were obtained. Thanks to the large chaotic variations in the flux, the “high” and “low” average levels differed by a factor of 1.5–2. Finally, for each observation the high-flux spectrum was divided by the low-flux spectrum to obtain a spectral ratio. A typical high-flux/low-flux spectral ratio is shown in Fig. 9 (from observation #4). A negative differential slope was obtained for all other observations within the outburst. It is evident from Table 5 that while spectral ratio slopes β_1 for separate sessions are not correlated with flux, high-to-low spectral ratios of a single observation always have slopes $\beta_2 < 0$. For comparison, we present in Fig. 9 the spectral ratio for Cyg X-1 calculated with the same technique. The effect is qualitatively the same for Cyg X-1 as for GS 1354–644, with a differential slope $\beta_2 = (-3.9 \pm 0.4) \times 10^{-2}$ (observation 26 June 1997).

We were concerned that selection effects might bias our estimates of β_2 . Because most counts fall in the soft part of the spectrum, one might get softer spectra simply by selecting for high flux, because we would be selecting for random excesses in the soft band. To check the importance of this effect, we changed our selection criteria and re-filtered the data

according to the flux levels above 10 keV. The results remained the same, indicating that the observed correlation of higher fluxes with softer spectrum was much stronger than any bias introduced by the selection criteria.

The systematic difference between high and low flux spectra can be interpreted in a variety of ways. The softening may be due to an increase in the relative contribution of shots that have a softer intrinsic spectrum than the constant flux. The constant flux, in turn, may be formed by the sum of shorter shots with harder spectra (this possibility is discussed, e.g. by Revnivtsev, Gilfanov & Churazov 1999). Another interpretation might be that the low energy shot emission changes the temperature of the hot plasma cloud responsible for Comptonization. Alternatively it might be suggested that the shot spectrum evolves with time and is softest near the maximum of the shot. Other explanations can not be excluded either.

Our spectral ratio analysis is quite sensitive to subtle changes in parameters of the system. We see that, in the course of the 1997 outburst, the spectrum softens steadily (except for observation #9). This implies that, in this case, the spectrum was not directly correlated with the flux level (or luminosity). We detected a hardness-flux anti-correlation for short-term flux variations within each observation, but not when we compared spectra for different observations. The last observation of the 1997 outburst, which breaks the overall pattern, likely corresponds to the secondary maximum or ‘kick’ in the light curve. The observation #10, performed a year after the maximum of 1997 outburst, showed a significantly softer spectrum with flux more than two orders of magnitude below the peak value.

5. Discussion

5.1. Spectral state

The high and low spectral states first identified in Cyg X-1 (Tananbaum et al. 1972) have since been observed in a number of X-ray binaries. The “high” and “low” terminology was originally chosen based on the 2-10 keV X-ray flux. It was later found that the *low* state corresponds to a hard spectrum, and the *high* state to a soft spectrum. A typical *high* state spectrum is the sum of a soft thermal component and a hard power-law tail. The *low* state spectrum is approximately power-law with an exponential cut-off at energies above ~ 100 keV. More detailed descriptions of the spectral states of X-ray binaries can be found elsewhere (e.g. Tanaka & Shibazaki 1996).

Studies of the aperiodic time variability in black hole candidates provided another

dimension to this phenomenology. In particular, a third very-high state has been recognized (Miyamoto et al. 1991, 1994; Ebisawa et al. 1994). This state is characterized by a 3-10 Hz QPO peak, plus either band-limited noise or a weaker power law noise component (Belloni et al. 1997).

The hard power-law-like energy spectrum with a slope ~ 1.5 that was detected from GS 1354–644 during its 1997 outburst is a clear indication of the low/hard spectral state. The character of the rapid variability, the absence of QPO, and the power spectrum of GS 1354–644 are similar to other black hole candidates in this state (Miyamoto et al. 1992; Nowak et al. 1999a; Nowak, Wilms & Dove 1999; Grove et al. 1998), and provide additional proof for such characterization. A similar time variability is manifested by neutron star binaries in their low state (Olive et al. 1998a; Ford et al. 1999). However, black hole systems in their other - high or very high - states have distinctly different power spectra (van der Klis 1995; Belloni et al. 1997).

GS 1354–644 was detected with Ginga in 1987 in its high/soft state (Kitamoto et al. 1990). But in 1997-1998 the same source was in a low/hard state. This confirms the earlier identification of the source as a black hole candidate and also demonstrates that both high/soft and low/hard states are generic for this group of X-ray sources. In fact, all the properties of GS 1354–644, that we revealed in our analysis are similar to other black hole candidates, both persistent and transient.

5.2. Geometry of the system

The energy spectrum of GS 1354–644 supports a model of low energy photons that are Comptonized in a hot plasma cloud. An accretion disk reveals itself via fluorescent iron line emission detected at ~ 6.4 keV and a reflected continuum detected at 15-20 keV. The equivalent line width and relative intensity of the reflected component are both consistent with reflection of harder X-ray emission from a cold plasma, which, in the commonly accepted model, is likely to be an optically thick accretion disk around the compact object. It is straightforward to assume that the X-ray source includes a cool disk plus a hot optically thick corona, which Comptonize the soft photons up to tens of keV. The exact geometrical configuration of the system remains uncertain.

This disk/corona combination is the most popular model for interpreting Galactic black holes in their low/hard spectral state. A slab geometry, where the accretion disk is sandwiched between two flat corona layers, was widely discussed several years ago (Haardt & Maraschi 1991, Haardt 1993), but cannot fit the spectra in a self-consistent manner

(see eg. Dove, Wilms & Begelman 1997). Other investigators have suggested a spherical hot corona (Kazanas, Hua & Titarchuk 1997) or an advection-dominated accretion flow (Narayan 1996) at radii smaller than the inner edge of the thick accretion disk. Seed soft photons could be generated in the accretion disk (Dove, Wilms & Begelman 1997, Dove et al. 1998) or inside the hot cloud (suggested by Narayan 1996 to be synchrotron/cyclotron photons). The former models invoke external illumination of the up-scattering region, while the latter invoke a source embedded inside the hot plasma.

The optical depth $\tau \sim 4 - 5$ inferred from our spectral fits (for *compST* and *compTT* models in a spherical geometry) is dependent both on the geometry and on the model, and hence can not be considered as a direct measurement of the optical depth. However, the value of τ indicates that the source of seed photons is most likely *inside* the hot cloud. In the case of external illumination of the Comptonization region by soft photons originating from the accretion disk, the optical depth parameter would be expected to be ~ 1 even for high intrinsic values of τ in hot cloud. A partial overlap of the disk by the corona may solve the puzzle, but the physical basis for such a configuration has yet to be explored.

If the characteristic frequency of the Compton cloud is the PDS break frequency about 2 – 3 Hz, then the cloud should be huge, which causes severe problems with energy balance (see e.g. Nowak et al. 1999a). More likely, the breaks in the PDS are determined by the intrinsic duration of the seed shots. They might also be related to the geometrical parameters of the system, such as the radius of the accretion disk, and with typical times, such as the plasma diffusion time. In the PDS of GS 1354–644 the first break frequency is anti-correlated with the flux, perhaps reflecting changes in some of the system parameters. For example, the inner edge of the disk is probably moving closer to the compact object when the mass accretion rate grows and the luminosity increases. Simultaneously the break frequency is decreasing, which might mean that shots become longer.

5.3. Dependence of fractional variability on energy

Fig. 4 shows that the integrated fractional variability of GS 1354–644 clearly decreases with energy. This decrease can be approximated by a power law $rms \sim E^{-0.07}$. Similar dependences have been found for Nova Per 1992 (Vikhlinin et al. 1995), Cyg X-1 (Nowak et al. 1999a), and GX 339–4 (Nowak, Wilms & Dove 1999), all Galactic black hole binaries, when observed in the low/hard state. In contrast, an *increase* of fractional variability with energy has been detected for X-ray bursters – e.g. 1E1724–3045 (Olive et al. 1998a), 4U1608–522 (Yu et al. 1997) in their low/hard state. This apparent difference between low-state black hole and neutron star systems is remarkable, because these

systems are otherwise so similar, when in their low/hard state. This fact motivated us to perform our own survey of publicly available RXTE data. The X-ray bursters 4U1705-44, SLX 1735-269, SAX J1808-3659, 4U1728-34 (GX 354-0) and 4U0614+091, together with the aforementioned systems 1E1724-3045 and 4U1608-522, were included in our analysis.

Power-law fits to the relation between *rms* variation and energy are presented on Table 6. All observations were taken when objects were in their low/hard state. For GX 339-4 and Terzan 2, the data were taken from Nowak, Wilms & Dove 1999 and Olive et al. 1998a respectively. Although a simple power law was in some cases a poor fit, we used it anyway to quantify the tendency (whether the *rms* variation decreased, increased or stayed constant with energy). Remarkably, slope is negative for all black hole binaries and positive for all neutron star binaries. The strongest correlation of fractional variability with energy is at energies below ~ 15 keV. In fact, the fractional variability has a broad maximum at energies 10-20 keV for many X-ray bursters, whereas for black holes the maximum is at the lowest observed energy. This might indicate that the similar spectra in black hole and neutron star systems have fundamentally different origins.

Whatever the physical reason, the difference is quite remarkable because of the substantial similarity in the other properties of black hole and neutron star systems in the low/hard state (e.g. Berger & van der Klis 1998; Revnivtsev et al. 1998; Olive et al. 1998a). If confirmed, this dependence may become an important new tool for deriving the type of compact object in Galactic binaries from X-ray observations.

6. Conclusions

We analyzed observations of the recurrent X-ray transient GS 1354-644 by the RXTE satellite. The observations were made during a modest outburst of the source in 1997-1998. The overall light curve was triangular with possible plateau at the maximum. PCA/HEXTE observations were carried out during both the rise and the decay phase of the outburst. The dramatic fast variability was studied in terms of a shot noise model. The power density spectrum can be approximated by the sum of 2 or 3 components, each corresponding to a specific type of shot. The most prominent components peak around 0.02–0.09 Hz and 2.3–2.9 Hz respectively. For several observations a third, intermediate component is statistically significant. Our flux density distribution analysis showed that the longest shots occur at a rate of 0.3 s^{-1} , and contribute 30–50% of the total flux. The short shots are more frequent ($\sim 10\text{--}15$ shots/s) and proportionally weaker, although their contribution to the total flux is comparable to the longer shots.

In general, the rapid time variability of the source X-ray flux is very similar to the low/hard state of other Galactic black hole systems, such as Cyg X-1, Nova Persei 1992, and GX 339-4.

The spectrum obtained by the PCA and HEXTE is clearly the hard/low state spectrum observed in many Galactic black hole binaries. The overall power-law-with-high-energy-cutoff shape can be approximated by Comptonization models based on up-scattering of soft photons on energetic electrons in a hot plasma cloud. In order to fit the data, an additional component describing a spectrum reflected from cold material with a strong iron fluorescent line must be included. Both the equivalent width of the line and the intensity of the reflected component are consistent with the assumption of the reflection of hard X-ray emission from a cold, optically thick accretion disk.

To examine finer spectral changes we analyzed ratios of the raw spectra. This technique demonstrated an overall softening of the spectrum during the outburst, except for the last observation, which was obtained during the secondary maximum. At shorter time scales, we detect a softening of the spectrum at higher flux levels.

An anti-correlation of fractional variability with energy is typical for Galactic black holes in their low spectral state (e.g. Nowak et al. 1999a, Vikhlinin et al. 1995, and this work), but a positive correlation is typical for neutron star systems in their low state (e.g. Olive et al. 1998a). Our analysis using RXTE archival data for several sources, confirmed this difference between black hole and neutron star binaries. This difference can be very useful for segregating neutron star binaries from black hole systems, which is otherwise difficult with X-ray data only.

The research has made use of data obtained through the High Energy Astrophysics Science Archive Research Center Online Service, provided by the NASA/Goddard Space Flight Center.

MR is thankful to Dr.M.Gilfanov for helpful discussions. KB is glad to acknowledge valuable comments by Prof.L.Titarchuk and Dr.S.Brumby. We are grateful to an anonymous referee for his/her careful comments on the manuscript, which helped us to improve the paper significantly.

REFERENCES

- Basko, M., Sunyaev, R., Titarchuk, L. 1974, A&A, 31, 249
- Barret, D., Grindlay, J.E., Harrus, I.M., & Olive, J.F. 1998, A&A, submitted, (astro-

ph/9810463)

- Belloni, T., & Hasinger, G. 1990, A&A, 230, 103
- Belloni, T., van der Klis, M., Lewin, W.H.G., van Paradijs, J., Dotani, T., Mitsuda, K., & Miyamoto, S. 1997, 322, 857
- Berger, M., & van der Klis, M. 1998, A&A, 340, 143
- Bradt, H.V., Rothschild, R.E., & Swank, J.H. 1993, A&AS, 97, 355
- Buxton, M., Vennes, S., Ferrario, L., & Wickramasinghe, D.T. 1998, IAU Circ.6815
- Castro-Tirado, A.J., Ilovaisky, S., Pedersen, H., Gonzalez, J.-F., Pizarro, M., Miranda, J., & Boehnhardt, H. 1997 IAU Circ.6775
- Chen, Wan, Shrader, C.R., & Livio, M. 1997, ApJ, 491, 312
- Dove, J.B., Wilms, J., & Begelman, M.C. 1998, ApJ, 487, 747
- Dove, J.B., Wilms, J., Nowak, M.A., Vaughan, B.A., & Begelman, M.C. 1998, MNRAS, 298, 729
- Ebisawa, K., Ogawa, M., Aoki, T., Dotani, T., Takizawa, M., Tanaka, Y., Yoshida, K., Miyamoto, S., Iga, S., Hayashida, K., Kitamoto, S., & Terada, K. 1994, PASJ, 46, 375
- Fender, R. P., Tingay, S. J., Higdon, J., Wark, R., & Wieringa, M. 1997, IAU Circ.6779
- Ford, E.C., van der Klis, M., Mendez, M., van Paradijs, J., & Kaaret, P. 1999, ApJL, 512, L31
- Francey, R.J. 1971, Nature Phys.Sci., 229, 228
- George, I.M., & Fabian, A.C. 1991, MNRAS, 249, 352
- Grove, J. E., Strickman, M. S., Matz, S. M., Hua, X.-M., Kazanas, D., Titarchuk, L., 1999, ApJ, 502, 45L
- Guainazzi, M., Parmar, A.N., Segreto, A., Stella, L., dal Fiume, D., & Oosterbroek, T. 1998, A&A, 339, 802
- Jahoda K. 1998a, <http://lheawww.gsfc.nasa.gov/users/keith/pcarmf.html>

- Jahoda K. 1998b, http://heawww.gsfc.nasa.gov/users/keith/pcarmf_ft41.erratum
- Haardt, F. 1993, *ApJ*, 413, 680
- Haardt, F., & Maraschi, L. 1991, *ApJ*, 380, L51
- Harmon, B.A., Zhang, S.N., Wilson, C.A., et al. 1994, in: *The 2nd Compton Symp.*, ed. C.E.Fichtel, N.Gehrels, & J.P.Norris (New York: AIP), 210
- Harmon, B.A., & Robinson, C.R. 1998, *IAU Circ.*6774
- Harries, J.R., McCracken, K.G., Francey, R.J., & Fenton, A.G. 1967, *Nature*, 215, 38
- Heindl, W., Blanco, P., Gruber, D., Pelling, M., Macdonald, D., Marsden, D., & Rothschild, R. 1997, *IAU Circ.*6790
- Kazanas, D., Hua, X.-M., & Titarchuk, L. 1997, *ApJ*, 480, 280
- Kitamoto, S., Tsunemi, H., Pedersen, H., Ilovaisky, S.A., & van der Klis, M. 1990, *ApJ*, 361, 590
- Lochner, J., Swank J., & Szymkowiak A. 1991, *ApJ*, 376, 295
- Lochner, J., & Roussel-Dupre, D. 1994, *ApJ*, 435, 840
- Magdziarz, P., & Zdziarski, A.A. 1995, *MNRAS*, 273, 837
- Makino, F. 1987, *IAU Circ.* 4342
- Markert, T.H., Canizares, C.R., Clark, G.W., Hearn, D. R., Li, F. K., Sprott, G. F., & Winkler, P. F. 1977, *ApJ*, 218, 801
- Mitsuda, K., Inoue, H., Koyama, K., Makishima, K., Matsuoka, M., Ogawara, Y., Suzuki, K., Tanaka, Y., Shibazaki, N., & Hirano, T. 1984, *PASJ*, 36, 741
- Miyamoto, S., Kimura, K., Kitamoto, S., Dotani, T., & Ebisawa, K. 1991, *ApJ*, 383, 784
- Miyamoto, S., Kitamoto, S., Iga, S., Negoro, H., & Terada, K. 1992, *ApJ*, L21, 391
- Miyamoto, S., Kitamoto, S., Iga, S., Hayashida, K., & Terada, K. 1994, *ApJ*, 435, 398
- Narayan, R. 1996, *ApJ*, 462, 136
- Nowak, M.A., Vaughan, B.A., Wilms, J., Dove, J.B., & Begelman, M.C. 1999a, *ApJ*, 510, 874
- Nowak, M., Wilms, J., Vaughan, B.A., Dove, J.B., & Begelman, M.C. 1999b, *ApJ*, preprint (astro-ph/9810406)

- Nowak, M., Wilms, J. & Dove, J. 1999, ApJ, preprint (astro-ph/9812180)
- Olive, J.F., Barret, D., Boirin, L., Grindlay, J.E., Swank, J.H., & Smale, A.P. 1998, A&A, 333, 942
- Olive, J.F., Barret, D., Boirin, L., et al. 1998, Submitted for publication in Advances in Space Research, Proc. of the 32nd COSPAR Meeting held in Nagoya, 12-15 July, 1998, "Broad band Spectra of Cosmic X-ray sources"
- Pedersen, H., Ilovaisky, S., & van der Klis, M. 1987, IAU Circ. 4357
- Pottschmidt, K., Wilms, J., Nowak, M.A., et al. 1998, to be published in "Highlights of X-Ray Astronomy, a symposium in honour of Joachim Truemper" (B. Aschenbach et al., eds.), MPE Report
- Rothschild, R.E., Blanco, P.R., Gruber, D.E., Heindl, W.A., Macdonald, D.R., Marsden, D.C., Pelling, M.R., Wayne, L.R., & Hink, P.L. 1998, ApJ, 496, 538
- Remillard, R., Marshall, F. & Takeshima, T. 1998, IAU Circ.6772
- Revnivtsev, M., Gilfanov, M., Churazov, E., & Sunyaev, R. 1998, To appear in Proc. of 3rd INTEGRAL Workshop (astro-ph/9812186)
- Revnivtsev, M., Gilfanov, M., & Churazov, E. 1999, A&AL, submitted
- Seward, F.D., Page, C.G., Turner, M.J.L., & Pounds, K. 1976, MNRAS, 177, 13
- Shakura, N.I., & Sunyaev, R.A. 1973, A&A, 24, 337
- Shakura, N., & Sunyaev, R. 1988, AdSpR, 8, 135
- Shapiro, S.L., Lightman, A.P., & Eardley, D.M. 1976, ApJ, 204, 187S
- Soria, R., Bessell, M.S. & Wood, P., IAU Circ.6781
- Stark 1998, <http://lheawww.gsfc.nasa.gov/~stark/pca/pcabackest.html>
- Sunyaev, R., & Shakura, N. 1986, SvAL, 12, 117
- Sunyaev, R.A., & Titarchuk, L.G. 1980, A&A, 86, 121 (ST80)
- Sunyaev, R.A., Borozdin, K.N., Aleksandrovich, N.L., Arefiev, V.A., Kaniovsky, A.S., Efremov, V.V., Maisack, M., Reppin, C., & Skinner, J.K. 1994, Astron.Lett., 20, 890
- Sutherland, P.G., Weisskopf, M.C., & Kahn, S.M. 1978, ApJ, 219, 1029

- Tanaka, Y., & Lewin, W.H.G. 1995, in *X-ray Binaries* eds. W.H.G.Lewin, J.van Paradijs, & E.P.J. van den Heuvel, Cambridge Univ.Press, 126
- Tanaka, Y., & Shibazaki, N. 1996, *Ann.Rev.Astron.Astroph.*, 34, 607
- Tananbaum, H., Gursky, H., Kellogg, E., Giacconi, R., & Jones, C. 1972, *ApJ*, 177, L5
- Terrell, N.J. 1972, *ApJ*, 174, L35
- Titarchuk, L.G. 1994, *ApJ*, 434, 570
- van der Klis, M. 1995, in *X-ray Binaries* eds. W.H.G.Lewin, J.van Paradijs, & E.P.J. van den Heuvel, Cambridge Univ.Press, 252
- van der Klis, M. 1989, in *Timing Neutron Stars*, H.Oegelman and E.P.J. van den Heuvel(eds.), Kluwer, Dordrecht (NATO ASI Series C 262), 27
- Vikhlinin, A., Churazov, E., Gilfanov, M., Sunyaev, R., Finoguenov, A., Dyachkov, A., Kremnev, R., Sukhanov, K., Ballet, J., Goldwurm, A., Cordier, B., Claret, A., Denis, M., Olive, J.F., Roques, J.P., & Mandrou, P. 1995, *ApJ*, 441, 779
- Wijnands, R., & van der Klis, M. 1998, preprint (astro-ph/9810342)
- Wilms, J., Nowak, M., Dove, J., Fender, R., Matteo, T. 1999, accepted in *ApJ* (see also astro-ph/9904123)
- White, N., Stella, L., & Parmar, A. 1988, *ApJ*, 324, 363
- Wood, K.S., Meekins, J.F., Yentis, D.J., Smathers, H.W., McNutt, D.P., Bleach, R.D., Friedman, H., Byram, E.T., Chubb, T.A., & Meidav, M. 1984, *ApJ Suppl.*, 56, 507
- Yu, W., Zhang, S.N., Harmon, B.A., Paciesas, W.S., Robinson, C.R., Grindlay, J.E., Bloser, P., Barret, D., Ford, E.C., Tavani, M., & Kaaret, P. 1997, *ApJ*, 490, L153
- Zhang, W., & Jahoda, K. 1996, <http://lheawww.gsfc.nasa.gov/users/keith/deadtime/deadtime.html>

Table 1: RXTE observations of GS 1354-644.

#	Obs. ID	Date	Start time	TJD ^t	Exposure, sec.	
					PCA	HEXTE ^d
1	20431-01-01-01	18/11/97	00:28:32	10770.019	1672	-
2	20431-01-02-01,3	19/11/97	13:11:28	10771.553	5920	1812
3	20431-01-03-00	22/11/97	09:39:28	10774.402	6592	2601
4	20431-01-04-00	05/12/97	05:00:48	10787.209	6809	2053
5	20431-01-05-00	12/12/97	19:21:20	10794.806	6119	1969
6	30401-01-01-00	27/12/97	14:39:28	10809.610	6516	1896
7	30401-01-02-00	04/01/98	17:47:12	10817.741	7349	2321
8	30401-01-03-00	12/01/98	15:04:32	10825.628	6355	1932
9	30401-01-04-00	26/01/98	12:07:28	10839.505	6594	2191
10	30401-01-05-00	17/11/98	10:00:14	11134.583	4109	1597 ^r

^d - Dead time corrected exposure for each cluster of HEXTE detectors.

^r - This observation was in real-time format, so we could not correct it for dead time

^t - TJD=JD-244000.5, where JD is Julian Date or number of days since Greenwich mean noon on Jan 1, 4713 B.C.

Table 2: Best-fit parameters for power spectra approximation (3–60 keV, 10^{-3} –20 Hz),

Obs.	rms_{total} %	$Break_1$ 10^{-2} Hz	rms_1 %	$Break_2$ Hz	rms_2 %	$Break_3$ Hz	rms_3 %	$\chi^2_{100dof}/100$
1	39.2 ± 2.6	8.2 ± 0.9	27 ± 2	0.39 ± 0.23	16 ± 6	2.31 ± 0.18	23 ± 1	1.4
2	32.5 ± 1.1	2.5 ± 0.2	16 ± 1	0.36 ± 0.05	15 ± 1	2.27 ± 0.10	20 ± 1	1.6
3	31.8 ± 1.3	2.6 ± 0.2	14 ± 1	0.47 ± 0.06	16 ± 1	2.55 ± 0.10	23 ± 1	1.2
4	31.5 ± 1.2	5.8 ± 0.4	18 ± 1	0.72 ± 0.17	12 ± 1	2.87 ± 0.16	23 ± 1	1.1
5	29.8 ± 1.2	7.5 ± 0.3	19 ± 1	-	-	2.30 ± 0.04	23 ± 1	1.5
6	29.4 ± 1.7	9.5 ± 0.3	19 ± 1	-	-	2.37 ± 0.05	23 ± 1	1.4
7	28.9 ± 2.3	9.6 ± 0.3	18 ± 2	-	-	2.48 ± 0.05	23 ± 1	1.2
8	33.2 ± 2.6	10.1 ± 0.3	23 ± 2	-	-	2.50 ± 0.06	24 ± 2	1.3
9	34.9 ± 4.1	9.1 ± 0.3	27 ± 2	-	-	2.27 ± 0.07	22 ± 2	1.2
10	< 25							

- The power spectrum was approximated by a three component model. Each component is a function $\sim \frac{1}{1+(\frac{f}{break_x})^2}$, corresponding to a simple exponential shot power spectrum. In the 6th–9th observations the intermediate component was not significant.

- The systematic uncertainty of the background rate was included when calculating the errors in the rms values of all components.

Table 3: Spectral fit parameters for GS 1354–644.

<i>Pexrav</i> (power law with cutoff + reflection) + Gauss ^d							
Obs.#	α	E_{cutoff} , keV	$\Omega/2\pi^a$		EW, eV	F ^b	$\chi^2_{324dof}/324$
2–5	1.52 ± 0.05	123 ± 8	0.56 ± 0.04		58 ± 12	59.5 ± 0.5	0.74
6–9	1.54 ± 0.07	230 ± 20	0.41 ± 0.04		53 ± 12	36.5 ± 0.04	0.99
Broken power law with cutoff + Gauss ^d							
Obs.#	α_1	E_{break} , keV	α_2	E_c , keV	EW, eV	F ^b	$\chi^2_{323dof}/323$
2–5	1.41 ± 0.02	10.1 ± 0.3	1.12 ± 0.02	57 ± 3	54 ± 12	58.7 ± 0.5	0.75
6–9	1.46 ± 0.02	10.4 ± 0.3	1.18 ± 0.02	84 ± 5	57 ± 12	36.3 ± 0.04	0.92
CompTT ^c + reflection + Gauss ^d							
Obs.#	kT_e , keV	τ	$\Omega/2\pi^a$		EW, eV	F ^b	$\chi^2_{324dof}/323$
2–5	28 ± 2	$2.1 \pm 0.1(\text{disk})$ $4.8 \pm 0.2(\text{sphere})$	0.29 ± 0.05		63 ± 15	57.5 ± 0.5	0.98
6–9	33 ± 2	$1.9 \pm 0.1(\text{disk})$ $4.3 \pm 0.2(\text{sphere})$	0.3 ± 0.07		57 ± 12	35.5 ± 0.5	1.1
CompST(sphere) + reflection + Gauss ^d							
Obs.#	kT_e , keV	τ	$\Omega/2\pi^a$		EW, eV	F ^b	$\chi^2_{324dof}/323$
2–5	23.6 ± 1.0	5.0 ± 0.1	0.55 ± 0.05		65 ± 12	54.3 ± 0.8	0.86
6–9	28.8 ± 1.0	4.5 ± 0.1	0.33 ± 0.05		50 ± 12	31.9 ± 0.8	0.92
Power law							
Obs.#	α	$F_{3-20keV}$	$F_{20-100keV}$				χ^2_{43dof}
10	2.0 ± 0.1	0.24 ± 0.04	< 1.2				0.64

^a - The error bounds do not include the potentially important effect of cross-calibration uncertainties between the PCA and HEXTE

^b - The source flux in the energy band 3–170 keV in units of 10^{-10} erg/s/cm². The HEXTE normalization was adjusted to the PCA

^c - For this model the optical depth was calculated for both sphere and disk geometries. The CompST model assumed a spherical geometry

^d - The width of the Gaussian line was fixed at 0.1 keV; $\cos(\theta)$ (θ - inclination angle) for the reflection component was fixed at the value 0.45

Table 4: Spectral fits to HEXTE data (20–170 keV).

Power law with cutoff			
Obs.#	α	E_{cutoff} , keV	χ^2_{282dof}
2–5	1.13 ± 0.04	66 ± 4	234
6–9	1.05 ± 0.05	80 ± 8	292

- different HEXTE clusters (detectors) were fitted with different normalizations

Table 5: Power-law fits to GS 1354–644 spectral ratios.

#Obs.	Flux/Flux _{ref} , %	$\beta_1^*, \times 10^{-2}$	χ^2_{44}	Flux _{max} /Flux _{min}	$\beta_2^*, \times 10^{-2}$	χ^2_{44}
1	88 ± 1	3.6 ± 0.3	0.74	1.97 ± 0.01	-5.7 ± 0.8	0.85
2	88 ± 1	4.6 ± 0.3	1.01	2.35 ± 0.01	-5.7 ± 0.8	1.00
3	98 ± 1	2.7 ± 0.2	0.70	1.86 ± 0.01	-5.7 ± 0.4	1.13
4	-	-	-	1.83 ± 0.01	-6.8 ± 0.7	1.18
5	89 ± 1	-0.3 ± 0.2	0.73	1.95 ± 0.01	-6.2 ± 1.0	0.91
6	69 ± 1	-1.7 ± 0.3	0.72	1.59 ± 0.01	-3.6 ± 0.7	0.95
7	54 ± 1	-1.7 ± 0.2	1.01	1.57 ± 0.01	-2.9 ± 0.7	1.16
8	51 ± 1	-1.9 ± 0.2	0.75	1.41 ± 0.01	-2.3 ± 0.7	0.79
9	59 ± 1	8.4 ± 0.5	1.06	1.70 ± 0.01	-22 ± 2	1.02
10	2.2 ± 0.3	-59 ± 6	0.55	-	-	-

* – β_1 is the power-law index of the spectral ratio for an individual observation normalized to observation #4. β_2 is the same parameter for ratio of high-flux and low-flux spectra within a single observation. The power-law indices β_1 and β_2 can be measured with very high accuracy as long as the instrument response is stable. Observations of the Crab nebula show that the slope of the spectrum is constant to $\sim 6 \times 10^{-3}$ for up to 5 months.

Table 6: Energy dependence of the rms fractional variability for Galactic X-ray binaries observed in low/hard state, expressed as a power law slope in the ~ 3 –15 keV energy range.

Source	Type	Date	PL slope
GS 1354-644	BH	Nov 19, 1997	-0.07 ± 0.01
Cyg X-1	BH	Jun 26, 1997	-0.05 ± 0.005
GX 339-4	BH	Sep 19, 1997	-0.035 ± 0.01^a
Terzan 2	NS	Nov 1996	$+0.25 \pm 0.04^b$
GX 354-0	NS	Mar 3, 1996	$+0.08^c$
SAX J1808.4-3658	NS	Apr 13, 1998	$+0.16 \pm 0.03$
4U1608-522	NS	Dec 27, 1996	$+0.6 \pm 0.3$
4U0614+091	NS	Jan 25, 1997	$+0.20 \pm 0.04$
4U1705-44	NS	Mar 29, 1997	$+0.13 \pm 0.05$
SLX 1735-269	NS	Feb-May, 1997	$+0.10 \pm 0.17$

^a - Nowak, Wilms & Dove 1999

^b - Olive et al. 1998a

^c - No confidence interval is quoted, because the rms variability dependence on energy does not fit a simple power-law (see Fig.4a)

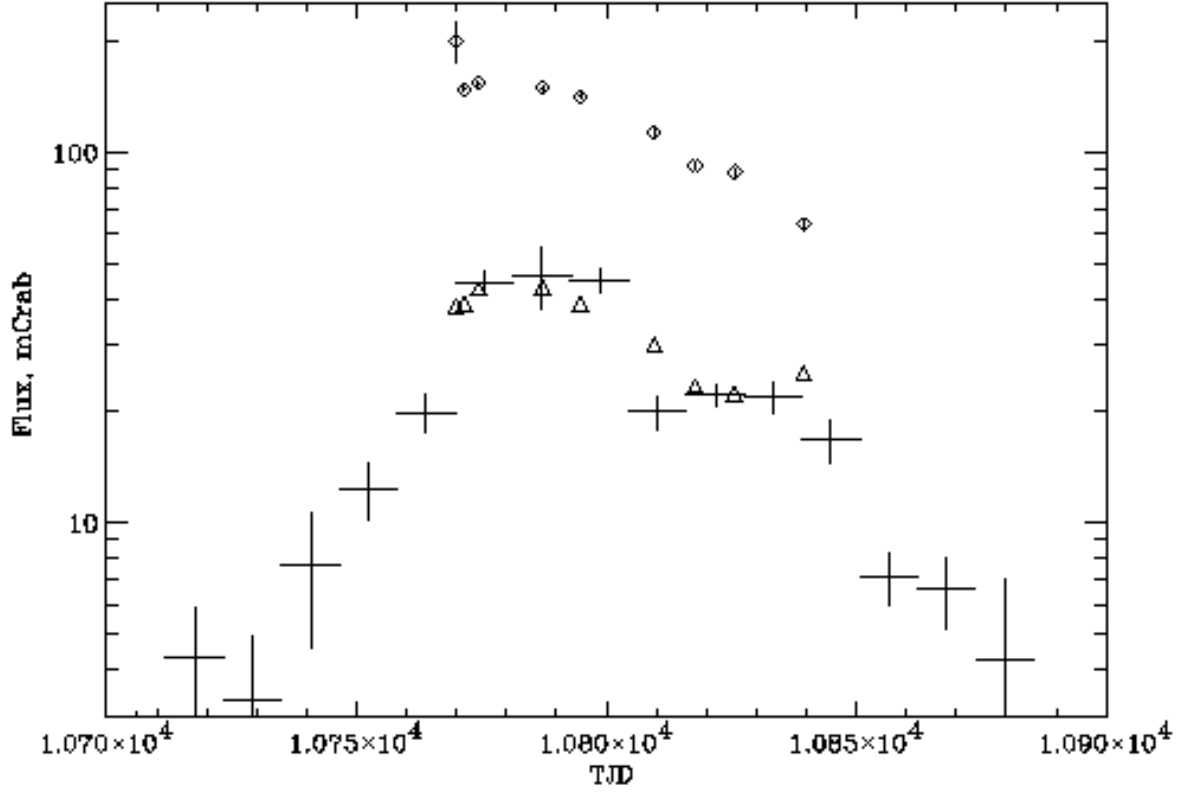


Fig. 1.— Light curve for the 1997-1998 outburst of GS 1354–644. Time axis in Truncated Julian Dates (TJD=JD-2440000.5). Crosses represent the ASM data (1.3–12.2 keV), open triangles - the PCA data (3–20 keV), and diamonds - the HEXTE data (20–100 keV), all normalized to the Crab nebula flux in the respective band.

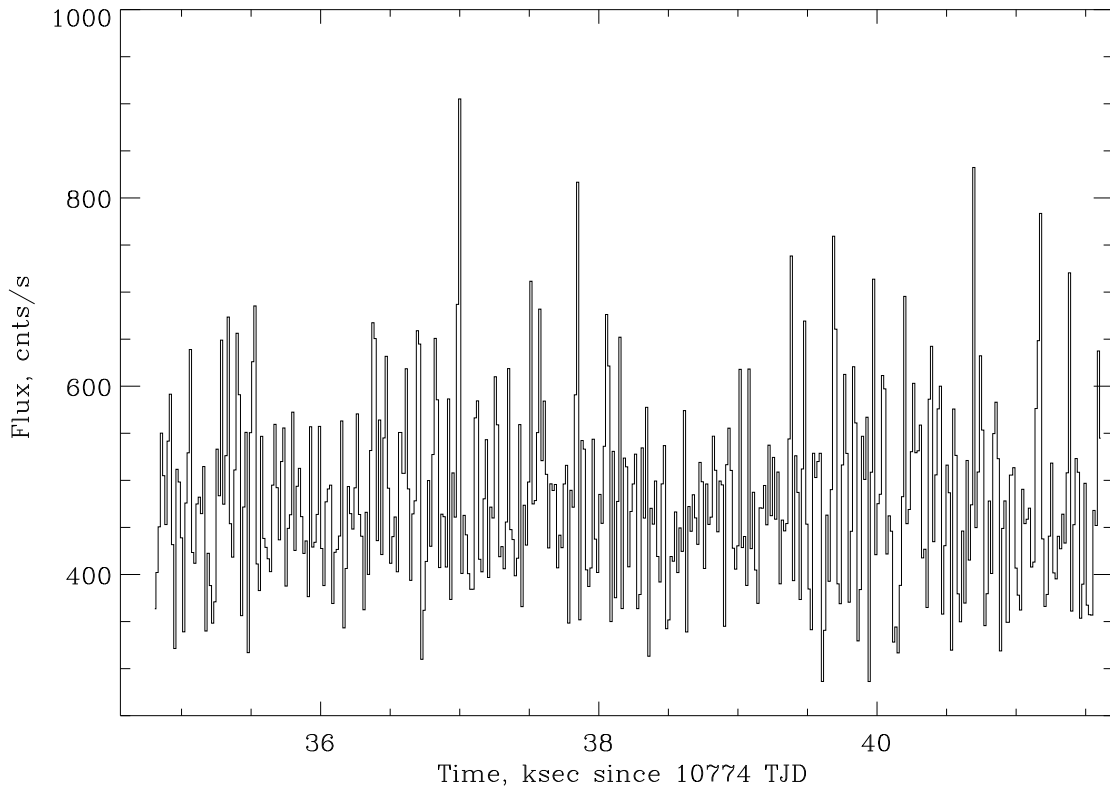


Fig. 2.— A typical time history of GS 1354–644, as observed by PCA. Each bin corresponds to a 16-sec time interval. Statistical errors are negligible on this scale.

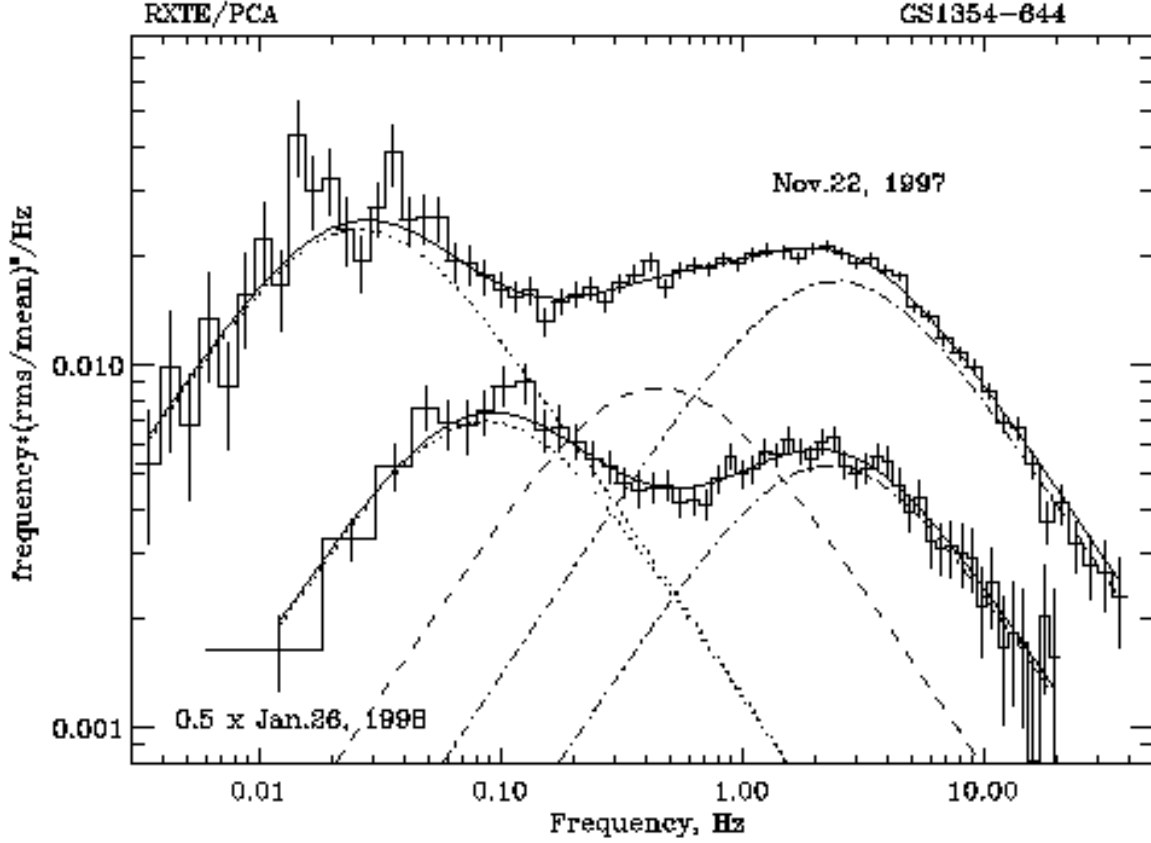


Fig. 3.— Power density spectra for two observations of GS 1354–644 with PCA. The upper spectrum was obtained for the observation #3; lower one for #9. Three model components (see Table 3 and text) are shown by dotted, dashed and dash-dotted lines respectively for both observations. The data and model for observation #9 (a two-component model was applied in this case) were multiplied by 0.5 to avoid confusion with observation #3.

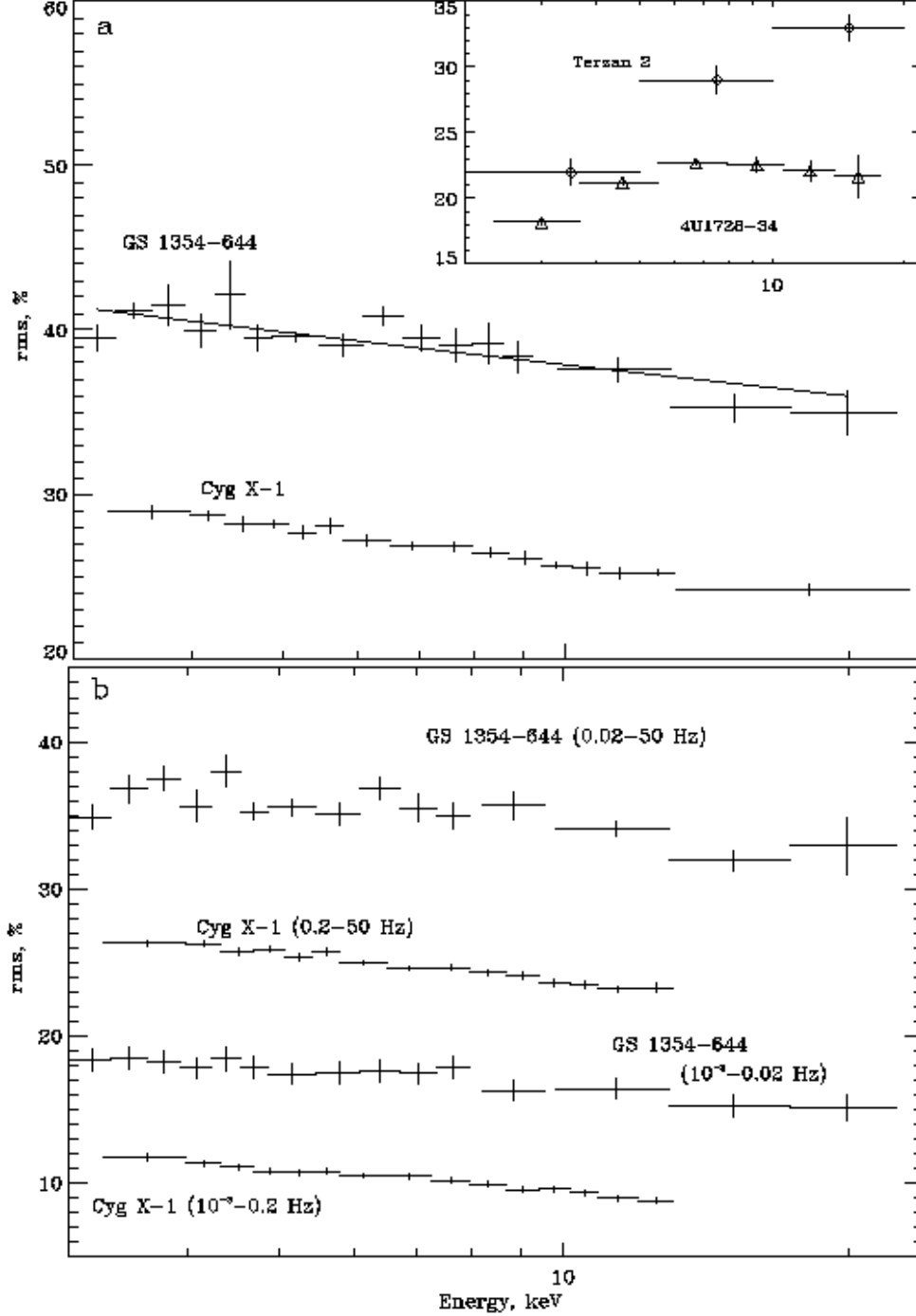


Fig. 4.— *Upper panel(a)*: The dependence of the fractional variability (% *rms*) of GS 1354–644 flux integrated over the frequency range 10^{-3} –40 Hz on photon energy (observation #3). Dependences for Cyg X-1, 4U1728-34 and Terzan 2 (Olive et al., 1998a) are also shown for comparison. *Lower panel(b)*: Energy dependence of the fractional variability (% *rms*) evaluated over different frequency ranges (above and below the first break in the PDS) for GS 1354–644 and Cyg X-1.

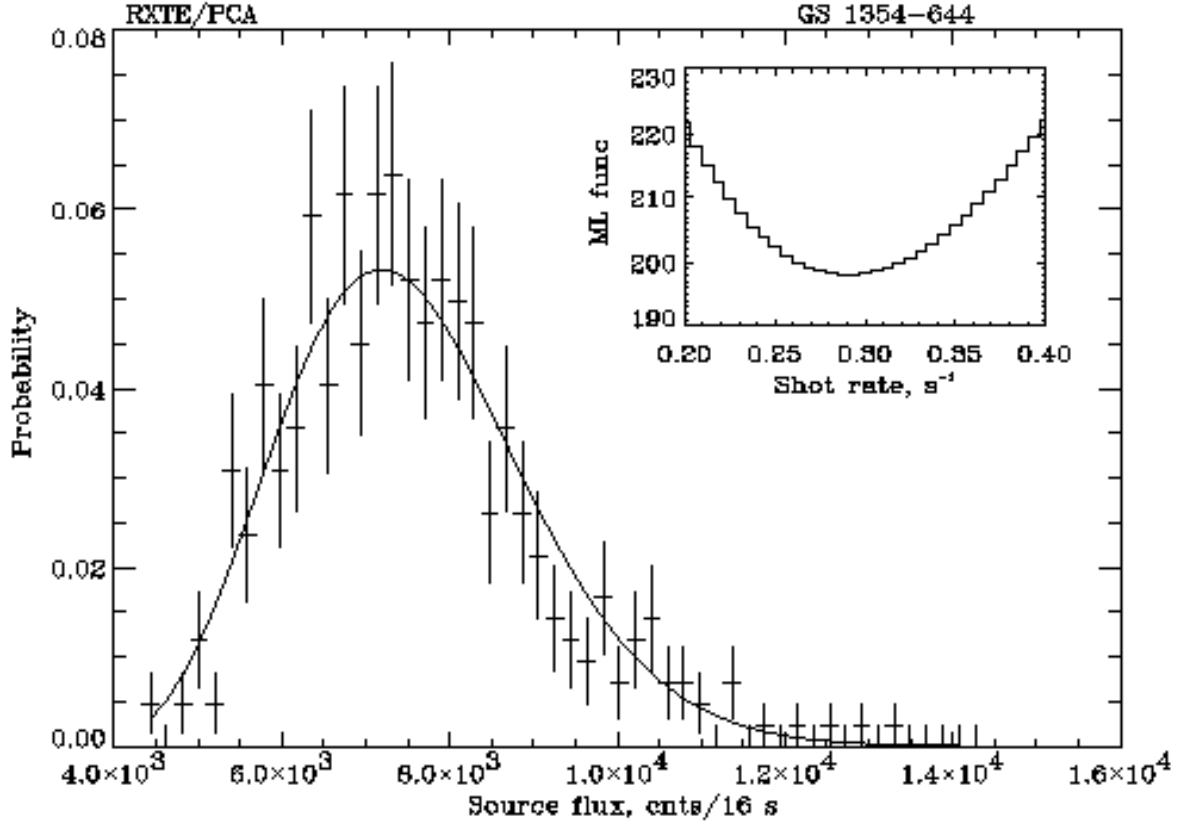


Fig. 5.— The distribution of the source flux integrated in 16-sec bins (observation #3). The dependence of the maximum likelihood function on shot rate is shown in the upper right corner. The best fit parameters are: a single shot amplitude ~ 215 counts and a shot rate of ~ 0.3 shots/s.

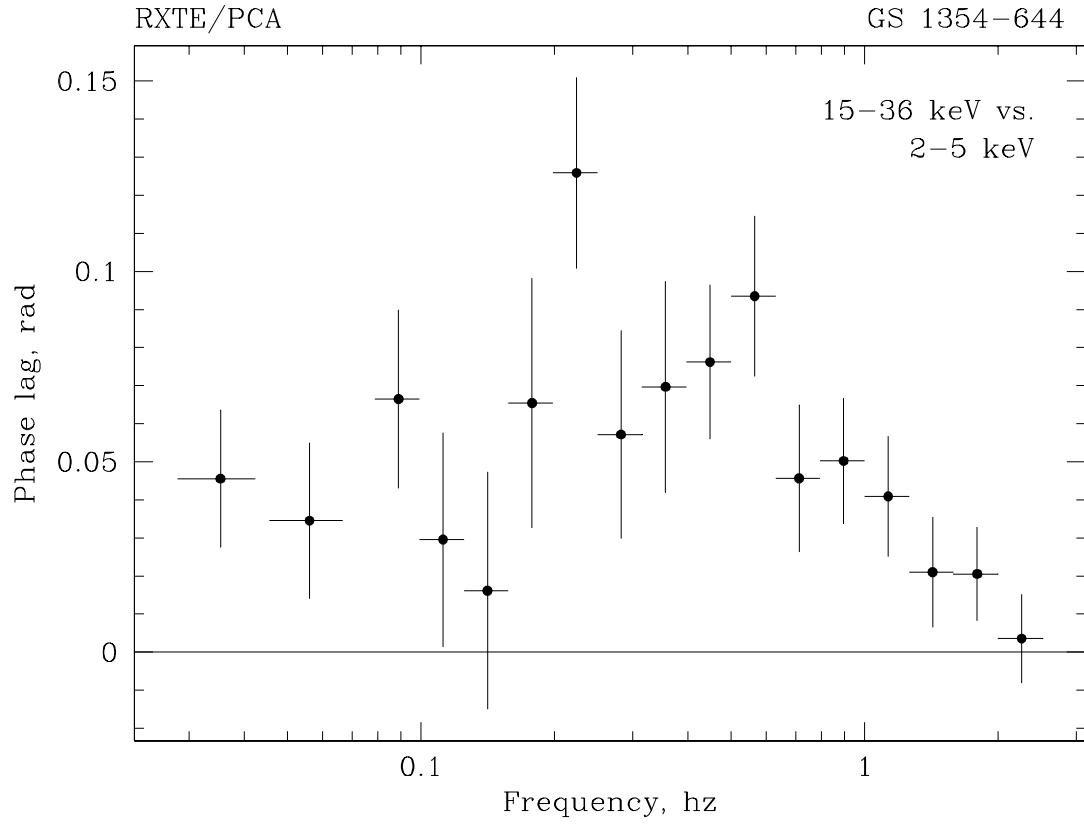


Fig. 6.— Phase lag as a function of Fourier frequency for the 15–36 keV energy band vs. the 2–5 keV energy band.

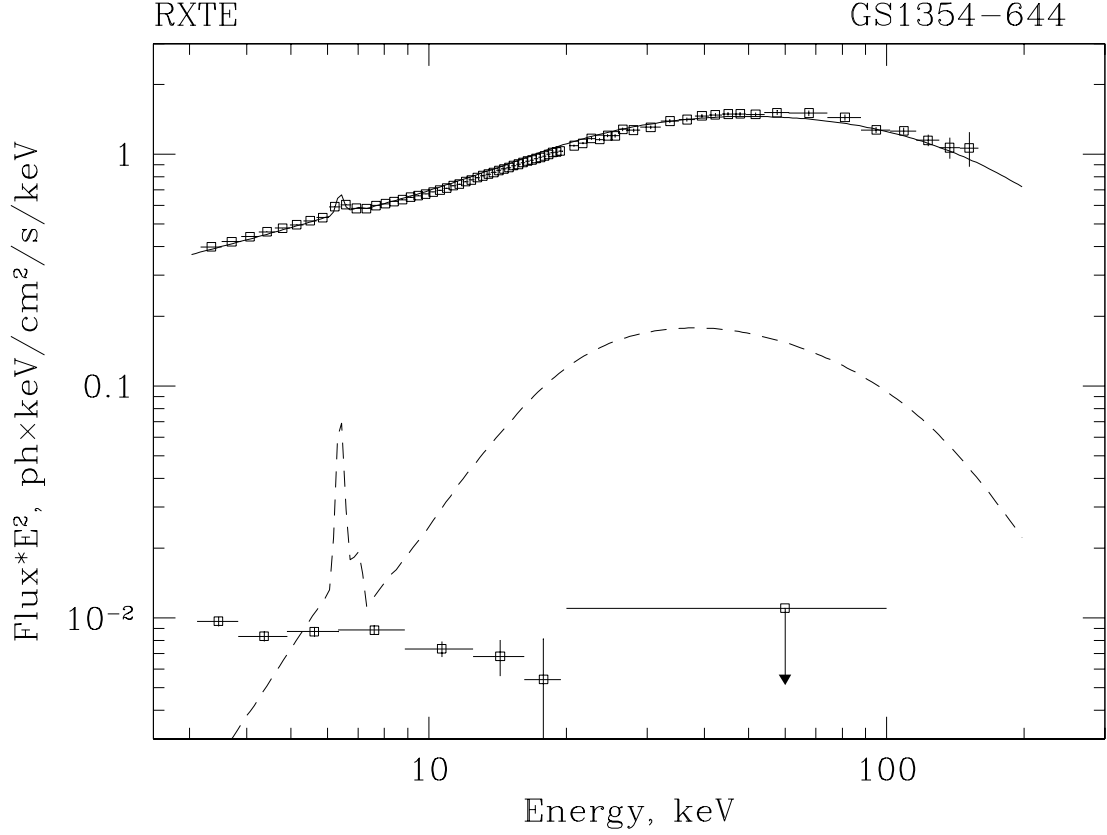


Fig. 7.— Spectral energy distribution of GS 1354-644 during the outburst maximum and in quiescence. The upper spectrum is an average over observations 2–5, and the lower one is from observation #10 (there was no detection by HEXTE, so a 2σ upper limit is shown for energies above 20 keV). The solid line is a spectral fit to the data by the model described in the text (*compST* + *reflection* + *Gauss*; see Table 3). The components produced by adjacent cold matter through Compton reflection and Fe K_{α} fluorescence are shown by the dashed curve.

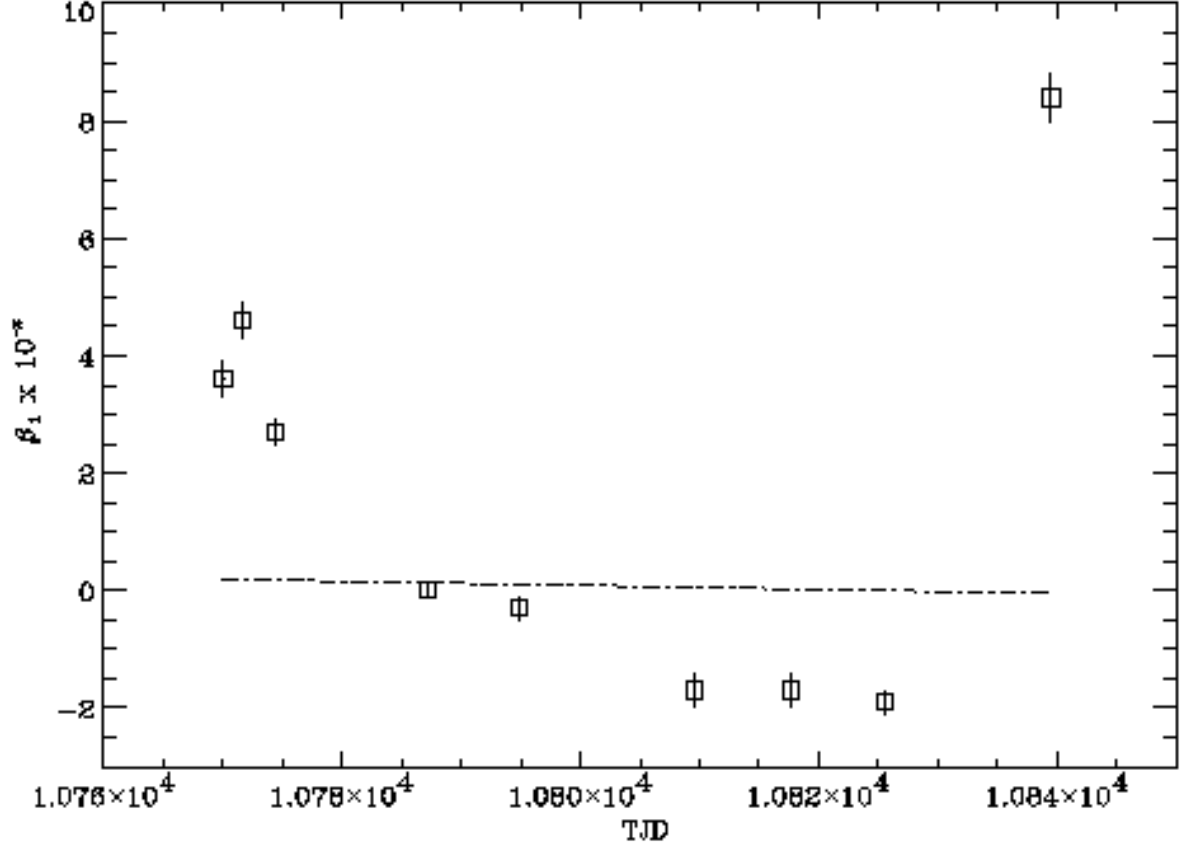


Fig. 8.— The evolution of the spectral ratio slope (see text) during the transient outburst. Observation #4 was used as a reference spectrum. The dot-dashed line shows the instrumental stability obtained from observations of the Crab nebula. We note an overall softening of the spectrum through observation #8. Observation #10, made a year later, is not shown.

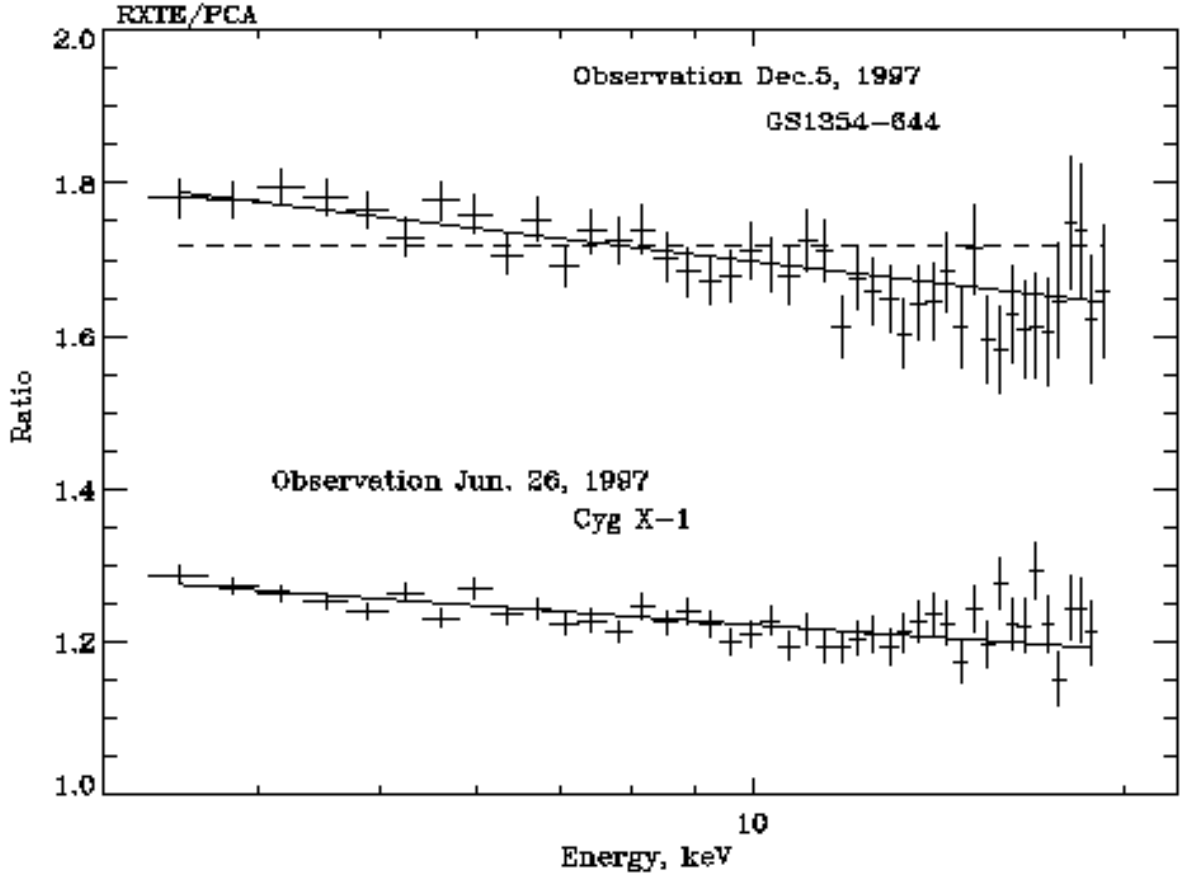


Fig. 9.— The 3-20 keV spectral ratio for GS 1354-644 (observation #4) obtained by segregating higher and lower flux intervals, as described in the text. A similar ratio for Cyg X-1 is shown for comparison. In both cases the spectrum softens at higher flux levels.